Target scattering or reflection is used by radar systems to identify and detect targets. The larger the echo that was returned to the radar receiver, the superior the signal-to-noise ratio and the greater the likelihood of detection. The radar cross-section (RCS) determines the quantity of energy reflected from a target in radar systems. This work shows new modeling for radar targets with growing stages of fidelity. We introduce the RCS concept for straightforward point targets and extend this into additional complex states of targets with several scattering midpoints. In addition, we discuss the modeling of fluctuations in RCS with time and briefly consider the case of the polarized signal. Because the receiver and transmitter are co-located, the effort focuses on narrowband mono-static radar techniques. The RCS value changes between scans. We simulate the replicated power of a sent signal over 10,000 scanning over unit incident signals, assuming that the signal illuminates the target just once each dwell. The target is modeled by four scatterers that are placed at four square vertices. All scatterers are cylindrical-point targets on a 0.5-meter square XY plane without losing generality. The acquired results demonstrated how to generate target echoes while accounting for statistical fluctuations. From the relation between RCS and elevation angle variations for cylindrical targets, the obtained result demonstrated that the first two outputs are the same and confirmed that there is no reliance on azimuth angle. The comparison between wideband and narrowband RCS patterns demonstrated that the RCS profiles of the target-matched shallower nulls for azimuth direction are in the range of (40–50) degrees at zero elevation for 4 scatterers' extended targets

Keywords: radar cross-section (RCS), target scattering, point targets, measured targets' profiles, extended targets

UDC 621
DOI: 10.15587/1729-4061.2022.265089

IMPLEMENTATION OF RADAR CROSS-SECTIONS MODEL FOR TARGETS WITH DIFFERENT SCATTERING CENTERS

Sameir Aziez
Doctor of Communication Engineering
Department of Electromechanical Engineering*
Ekhlas Hamza
Doctor of Electric Engineering/Communications
Department of Control and Systems Engineering*
Fadia Hummadi
Doctor of Electric Engineering/Communications
Department of Communications
Al-Khwarizmi Collage of Engineering –
University of Baghdad
Al Jadriyah Bridge, Baghdad, Iraq, 64074
Ahmad Sabry
Corresponding author
Doctor of Control and Automation Engineering
Department of Computer Engineering
Al-Nahrain University
Al Jadriyah Bridge, Baghdad, Iraq, 64074
E-mail: ahs4771384@gmail.com
*University of Technology – Iraq
Al-Sina'a str., Baghdad, Iraq, 10066

Received date 08.07.2022
Accepted date 15.09.2022
Published date 27.10.2022

How to Cite: *Aziez, S., Hamza, E., Hummadi, F., Sabry, A. (2022). Implementation of radar cross-sections model for targets with different scattering centers. Eastern-European Journal of Enterprise Technologies, 5 (9 (119)), 54–60. doi: https://doi.org/10.15587/1729-4061.2022.265089*

1. Introduction

The radar emits an electromagnetic wave and the microwave region of the electromagnetic spectrum. The little arrows coming off the target represent the electromagnetic radiation scatters off of all the different scattering centers. A radar cross-section (RCS) is simply an effective electrical area that the target sees, by which the energy that hits that electrical area is scattered back to the radar. To provide background and some definitions of the RCS, Fig. 1 shows a simple representation of a radar operation.

Therefore, it is important to obtain the dimensions of that area and calculate the amount of the reflected energy. Moreover, RCS is the area intercepting the amount of energy, which, if radiated isotropically, produces the same received energy in the radar [1–3].

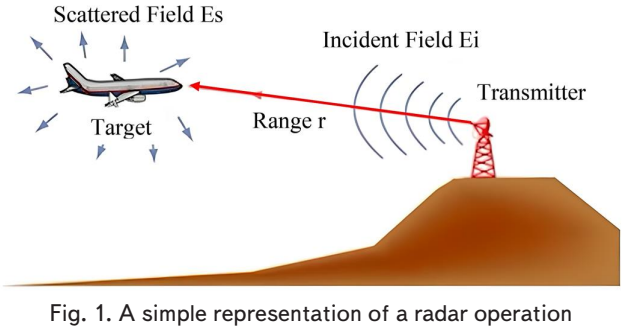

Fig. 1. A simple representation of a radar operation

One of the crucial factors in the target detection process is the radar cross-section [4]. It is used to describe the strength of the scattered radar power coming from a target. Low RCS must be maintained in stealth designs for aircraft

and seacraft. The detectability decreases when the RCS increases, and vice versa. In traditional aircraft, a larger aircraft has a greater RCS value. RCS is influenced by a number of factors, including the target's size, polarization, frequency, and aspect angle. RCS is primarily used by radar systems as a discrimination technique. Its forecast is crucial as a result. RCS can be decreased by measuring and locating the scattering centers for a certain target [5].

The characteristics of the RCS of ideal traffic contributors will significantly affect how well the real environment is recreated for an automotive millimeter-wave radar road scenario simulation. It is an ordinary practice to assess RCS in an anechoic chamber during the road set-up simulation test of superior driving support systems by utilizing vector network analyzers to create RCS models of typical traffic participants. However, using only one point to correspond to the RCS characteristics of typical traffic contributors is challenging because of the presence of multi-scattering midpoints of composite targets, which results in mistakes when compared to the real targets [6]. The position and brightness of the scattering centers of a radar target are described in RCS images, but the underlying scattering mechanisms are not disclosed [7]. As soon as it becomes accessible, this information may be of great assistance in designing radar targets. Volume decorrelation is now a controversial topic in synthetic aperture radar interferometers. It results from the height distribution of the backscattering cross-section in an imaged scene and has a significant impact on interferometric coherence images, such as when there are trees or structures present.

The appeal of this reduction comes from the possibility that resolving volume decorrelation and pinpointing the precise location of the scattering midpoints within resolution cells will enable us to estimate the height of the experiential spread scatterers. Both the development of digital elevation models and the assessment of biomass depend on the determination of the volume scattering contribution. The mechanisms that cause volume decorrelation, however, may be revealed by the phenomenon itself [8–10].

Therefore, research on the development to model radar cross-sections for targets with different scattering centers, including point targets, measured targets' profiles, and extended targets models, and to explain target echoes for statistical volatility is relevant.

2. Literature review and problem statement

Radar systems have been invented in numerous sectors, including land, marine, and even air, and their applications have grown throughout time. In [11], a strategy for suppressing height ambiguity based on bi-frequency and averaging multi-frequency interference was suggested. Although the study investigated the discrimination of scattering processes using polar imaging RCS and suggested a polarization technique to find and describe three separate scattering mechanisms regardless of scattered direction, the paper didn't analyze multiple scatterers' RCS of extended targets. This was discussed in [7], but because there is no knowledge about the underlying scattering processes, the approximation accuracy is restricted. The work [12] employed the synthetic aperture radar (SAR) approach to decrease clutter in the search by measuring the RCS. First, two two-dimensional radar pictures of the target were acquired by scanning the antenna twice linearly at different heights. The radar picture data were then used to derive the amplitude and phase of the scattering centers. Although the RCS of the target was constructed in this manner after filtering to eliminate clutter and increase RCS data accuracy, the scattering intensity was not sufficiently matched to the target. The determination of the contribution of size distribution is a limiting element in both the development of the digital elevation model and the assessment of biomass. However, this work didn't compare wideband and narrowband RCS patterns at zero elevation for 4 scatterers' extended targets. The behavior of the volumetric decorating connection owing to random sizes and fixed dispersed aims were distinguished in [8]. However, the study couldn't apply target fluctuation RCS histogram of target reflected signal.

In [13], an airborne synthetic aperture radar (SAR) was simulated to confirm the findings of a prior phenomenological study of the polarimetric vessel dispersal capacities of categorization algorithms that give satisfactory performance in congested settings. However, this paper didn't visualize the impact of elevation angle on the RCS pattern for a cylindrical target. The reference [5], on the other hand, deals with the investigation of the features of the radar cross-section in the stealth design of aircraft, where the remote control system (RCS) was dependent on numerous elements such as side angle, frequency, polarization, and target size. The RCS of triangular plate, spherical, cylindrical, and elliptical objects with dimension angle, frequency, and object dimensions were computed numerically. However, in order to determine RCS variance, they used a few items of regular shape. Although the RCS of triangular plate, spherical, cylindrical, and elliptical objects with dimension angle, frequency, and object dimensions were computed numerically, the study couldn't compare wideband and narrowband RCS patterns at zero elevation for 4 scatterers' extended targets. The work [6] investigated RCS estimate and synthesis of ideal traffic contributors, where a vector system analyzer was employed to construct RCS networks for ideal traffic contributors. When RCS systems are employed directly in the simulation test, the accuracy is low because of the significant oscillation of the targets. To increase the accuracy of the target simulation, the RCS synthesis and estimate approach for model traffic participants was presented. However, this research also didn't discuss the different scattering centers, including point targets, measured targets' profiles, and extended targets models.

Therefore, all this allows us to argue that it is appropriate to conduct a study devoted to producing target echoes while accounting for statistical volatility and formulate extended targets, point targets, and measured targets' profiles.

3. The aim and objectives of the study

The aim of the study is to develop modeling of radar cross-sections for targets with different scattering centers, including point targets, measured targets' profiles, and extended targets models, and to explain how to produce target echoes while accounting for statistical volatility. This will make it possible to identify and detect targets in wideband and narrowband RCS patterns of the target reflected signal.

To achieve this aim, the following objectives are accomplished:

– to visualize the impact of elevation angle on the RCS pattern for a cylindrical target;

– to analyze multiple scatterers' RCS of extended targets;

– to compare wideband and narrowband RCS patterns at zero elevation for 4 scatterers' extended targets;

– to apply target fluctuation RCS histogram of target reflected signal.

4. Materials and methods

4. 1. Object and hypothesis of the study

This work presents an implementation of a radar cross-section model for targets with different scattering centers. It explains RCS for straightforward point targets before extending it to additional challenging situations, including a target of many scattering midpoints. Additionally, the work describes the RCS's variations over time and partially addresses the polarized signal issues. Target detection and identification are done by a radar system using target scattering or reflection. The radar receiver receives a larger returning echo the more strongly a target reflects, increasing the signal-to-noise ratio (SNR) and the likelihood of detection.

The radar cross-section (RCS), represented by σ, in radar systems determines how much energy is reflected off a target, which is identified, in terms of the distance to the radar (R), the field strength of the target signal incident (E_i), and the field strength of the target reflected signal (E_s) by:

$$\sigma = \lim_{R\to\infty} 4\pi R^2 \frac{|E_s|^2}{|E_i|^2}.$$

Targets typically disperse power in every direction. The RCS depends on the frequency of the signal, the angle of scattering, and the angle of incidence [14]. RCS is influenced by the materials used and the target's shape in its construction. RCS frequently uses dBsm or square meters as a unit of measurement. This work focuses on narrowband mono-static radar systems with co-located receivers and emitters. The incident angle alone determines the RCS, and the scattered angles and the incident are equal, which is called the backscattered case. The signal bandwidth for narrowband radar is low in relation to the working frequency and is consequently thought of as a constant value.

4. 2. Point target radar cross-section

An isotropic scatterer serves as the most basic target model [15, 16]. A metallic sphere with a uniform density serves as an illustration of an isotropic scatterer. The incidence angle has no bearing on the reflected energy in this instance. An additional complicated point target, which is located far away from the radar, can frequently be approximated by an isotropic scatterer at the first order. For instance, an isotropic scatterer of 1 m^2 RCS can be used to imitate a pedestrian. Suppose that the operating frequency and propagation speed of the radar system are (Fc=3e+8, c=3e+8).

For input incident signal (x=1), the scattered signal is calculated using the MATLAB function «*pedestrian*(x)», which is obtained equal to 3.5449. The relation of the reflected incident signal, represented by the dimensionless gain (G) and operating frequency wavelength (λ), is given by:

$$y = \sqrt{G} * x, \text{ where } G = \frac{4\pi\sigma}{\lambda^2}.$$

There aren't many target shapes for which analytic RCS patterns may be determined. The RCS pattern can be precisely predicted for more complex forms and materials using computational electromagnetic techniques like finite element analysis (FEM) or methods of moments (MoM). The work [17] provides a more thorough overview of these methods. It is possible to input the results of these computations into the newly constructed object.

4. 3. Complex targets radar cross-section

It is no longer possible to regard reflections to be uniform in all directions for targets with more complicated geometries [18]. The aspect or incident angles affect the RCS differently. Like antenna radiation patterns, aspect-dependent RCS patterns can be modeled or measured.

The RCS values are represented in terms of elevation and azimuth angles in the local coordinate system of the target as the result of such models or measurements. As a function of elevation and azimuth angles, the scenario primarily calculates the RCS profile of a target with a cylindrical shape of 10 meters in height and a radius of 1 meter, which is not dependent on azimuth since the cylinder is z-axis symmetrical. Only elevation angle has an impact on RCS readings.

4. 4. Multiple Scatterers radar cross-section of Extended Targets

Despite the fact that computational electromagnetic techniques can produce precise RCS estimation, it frequently needs a large quantity of calculation and isn't appropriate in real-time models. Modeling a complicated target as a collection of basic scatterers is an alternate method for describing complex targets. The RCS profiles of the simple scatterer (σ_p) can then be used to determine the RCS pattern of the complicated target (σ) as in [1], as described here:

$$\sigma = \left| \sum_p \sqrt{\sigma_p} e^{j\theta_p} \right|^2,$$

where θ_p is the corresponding phase for the scatterer of order *pth*. An antenna array performs very similarly to a multi-scatterer target. The procedure for modeling a target with four scatterers is shown in Fig. 2.

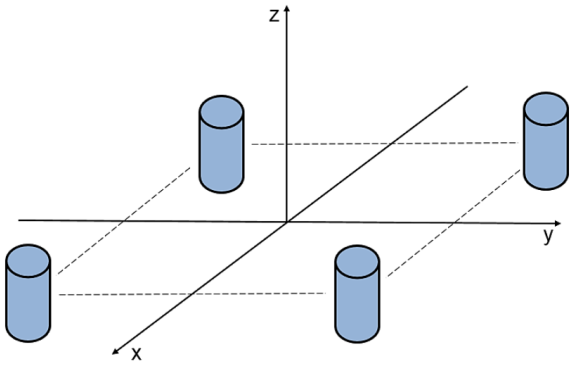

Fig. 2. Modeling of a target with four scatterers

At each of a square's four vertices there are the scatterers. As determined in the previous section, every scatterer was a point target of cylindrical shape. The square is positioned in the *XY* plane to maintain generality. The square has sides that are 0.5 meters long.

4. 5. Multiple scatterers wideband radar cross-section of Extended Targets

The standard definition of a wideband radar system is one with a bandwidth greater than 5 % of the central frequency.

Wideband systems provide better target detection in addition to enhanced range resolution. Loading in fades in an RCS profile of a target is one method wideband systems enhance detection performance. The extended target with four-cylinder scatterers from the earlier section can be used to illustrate this. It is assumed that azimuthal sweep across the target=–90:90.

We'll then look at the RCS profile with a wideband model using a similar middle frequency. This system's bandwidth will be positioned at 10 % with respect to the middle frequency and will be more than 5 % of the middle frequency. bw=0.10*fc and fs=2*bw follow from this.

As was done before for the extended target with narrowband, a wideband RCS model is developed. Radar engineers frequently receive RCS models that have been created offline using simulation software or range measurements to employ in the model systems. It is implicit in this case that the RCS modeling supplied was sampling on 1 MHz periods from the radar's center frequency side. Therefore, the model frequencies=(–80e+6:1e+6:80e+6)+fc.

The target RCS value is assumed to be constant over time in all the above discussions. In a real case, the RCS value fluctuates over time since both the target and the radar system are in motion. The target in this scenario changes over time. Peter Swerling created four numerical algorithms, known as Swerling one throughout Swerling four. They are commonly used in experiments to simulate variable targets.

All the proposed model simulations of the radar cross-section for targets with different scattering centers have been implemented using MATLAB.

5. Results of the radar cross-sections for targets with different scattering centers

5. 1. Impact of elevation angle radar cross-section patterns for a cylindrical target

The RCS profiles of a cylindrical target showing the impact of elevation angle are given in Fig. 3, while the relation between RCS and elevation angle variations for a cylindrical target is shown in Fig. 4.

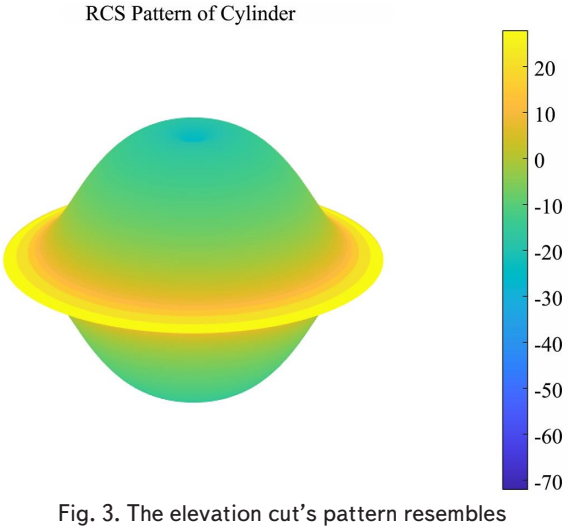

Fig. 3. The elevation cut's pattern resembles

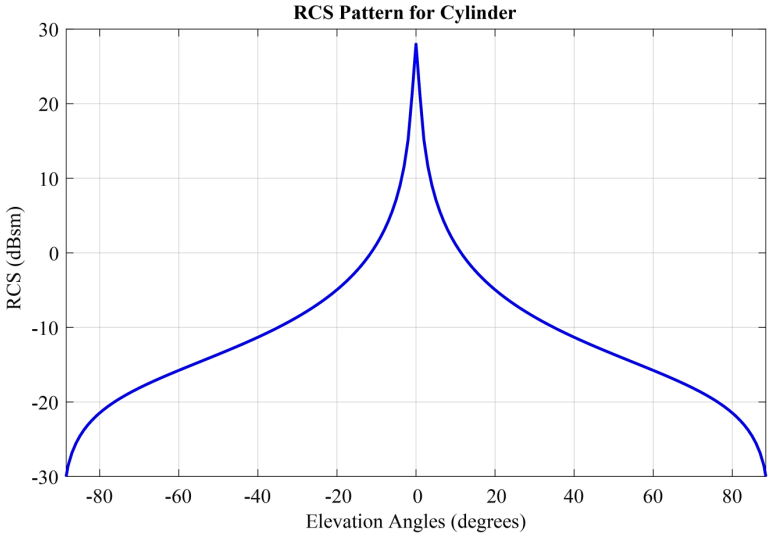

Fig. 4. The relation between radar cross-section and elevation angle variations for a cylindrical target

The target reflection is created after importing the RCS aspect-dependent profiles to a code object. It is assumed that the target reflects three identical signals on three distinct aspect angles. The primary two angles are with different azimuth angles but the same elevation angle. In comparison to the first two, the last has a distinct elevation angle. Therefore, three signals with unity values are represented by the vector x=[1 1 1], while the directions matrix is [0 30 30; 0 0 30]. The obtained result is [88.8577 88.8577 1.3161], which demonstrates that the first two outputs are the same and confirms that there is no azimuth angle dependence.

5. 2. Multiple Scatterers radar cross-section of Extended Targets

The scatterers' positions are defined by the matrix [–0.5 –0.5 0.5 0.5; 0.5 –0.5 0.5 –0.5; 0 0 0 0]. The incident angle of every element scatterer was similar if the target is in the transmitter's far field. The overall RCS pattern can then be calculated using the equation in the corresponding section in Methodology. The visualization of the RCS profiles of 4 scatterers for an extended target is shown in Fig. 5.

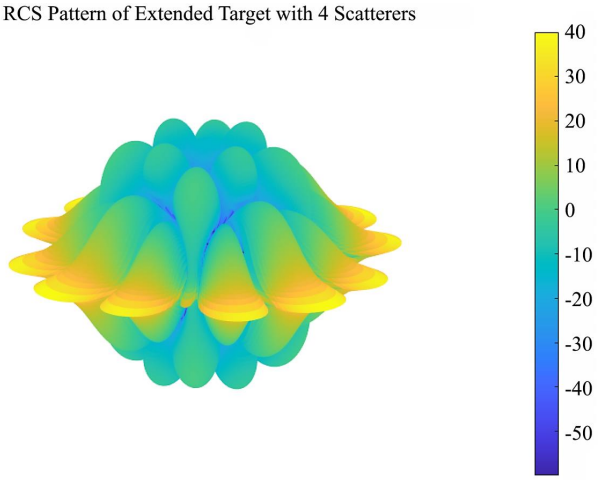

Fig. 5. Radar cross-section profiles of 4 scatterers for an extended target

These profiles can then be utilized in the previously created radar *Target* object to calculate the reflected power of the target signals. The obtained values are [355.4305 236.7634 0.000]. This result confirms that the signal reflected power relies on both angles of elevation and azimuth directions.

5. 3. Extended Targets Multiple radar cross-section for Wideband Scatterers

The extended target with four-cylinder scatterers from the earlier section can be used to illustrate this. It is assumed that the azimuthal sweep across the target=−90:90. Fig. 6 displays the modeled narrowband RCS swept across several target characteristics. Deep fades between 40 and 50 degrees are produced by the coherent combination of returns from various cylinders in the extended target model. The target may not be picked up via the sensor of the radar as a result of these fades.

The different distribution centers' contributions are formed similarly to earlier. It is significant to observe that, for this configuration, this estimate presupposes that each of the scattering centers of targets falls inside a similar variety bin resolution.

Now, utilizing the recently calculated RCS patterns, the RCS target wideband model is produced. After the wideband RCS has been modeled, the narrowband system can be compared as depicted in Fig. 7.

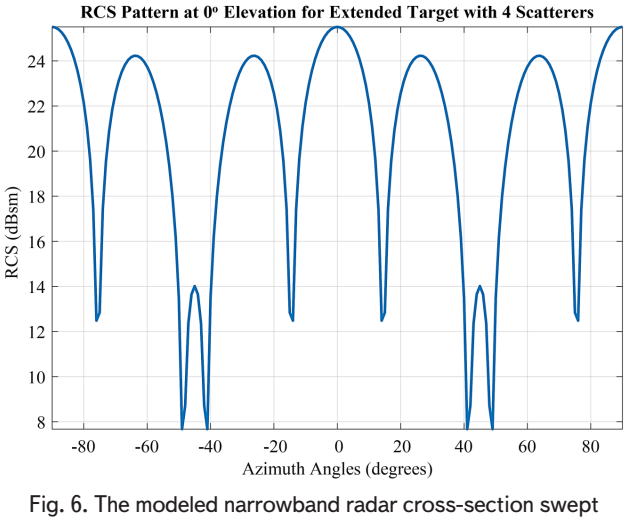

Fig. 6. The modeled narrowband radar cross-section swept across several extended target characteristics with 4 scatterers

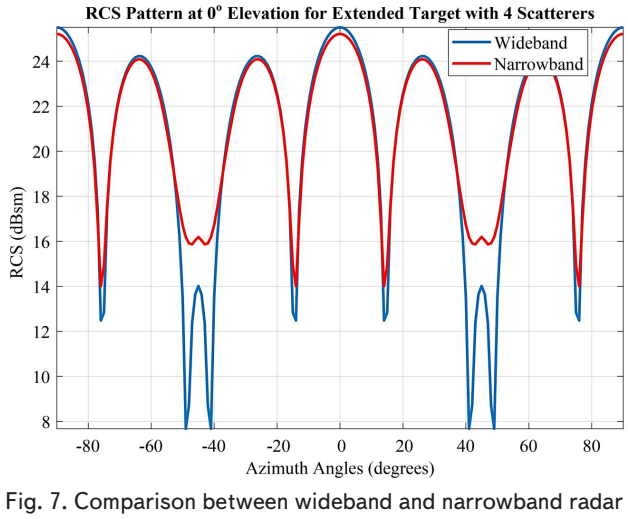

Fig. 7. Comparison between wideband and narrowband radar cross-section patterns at zero elevation of 4 scatterers extended target characteristics

These fades are filled in by the wideband waveform because, while several frequencies may encounter nulls for a particular feature, the bandwidth's vast bulk didn't at that azimuth angle.

5. 4. Target Fluctuation radar cross-section

The following table (Table 1) illustrates how the Swerling model divides unpredictable targets of two time-varying behaviors and two probability distributions.

Table 1

The division of unpredictable targets into two time-varying behaviors and two probability distributions by the Swerling model

Type of unpredictable targets	Fast Fluctuating	Slow Fluctuating
4^{th} Degree Chi-square	Swerling 4	Swerling 3
Exponential	Swerling 2	Swerling 1

During a dwell, a target's RCS with slow-fluctuating continues constant, yet it changes every scan. On the contrary, the target RCS with rapid variation shifts with each pulse throughout the course of a dwell. The equation of Swerling 2 and 1 follows a pdf (exponential density function), which is written as:

$$p(\sigma)=\frac{1}{\mu_\sigma}e^{-\sigma/\mu_\sigma}.$$

These models can be used to simulate a target made up of a number of scatterers of similar strengths. For Swelling 4 and 3, the equations follow a Chi-square pdf with 4^{th} degree, which is written as:

$$p(\sigma)=\frac{4\sigma}{\mu_\sigma^{\,2}}e^{-2\sigma/\mu_\sigma}.$$

When the target has a dominant scattering component, these models are applicable. μ_σ indicates the RCS mean value and represents the RCS quantity for the identical targets within the non-fluctuating supposition, in both pdf definitions. The Swerling 1 statistical model is applied to generate the radar echo from the previously discussed cylindrical target.

The previously determined non-fluctuating RCS is used in the theoretical prediction. For the cylindrical target, Fig. 8 shows the reflected signal power at normal incidence for a unit power input signal.

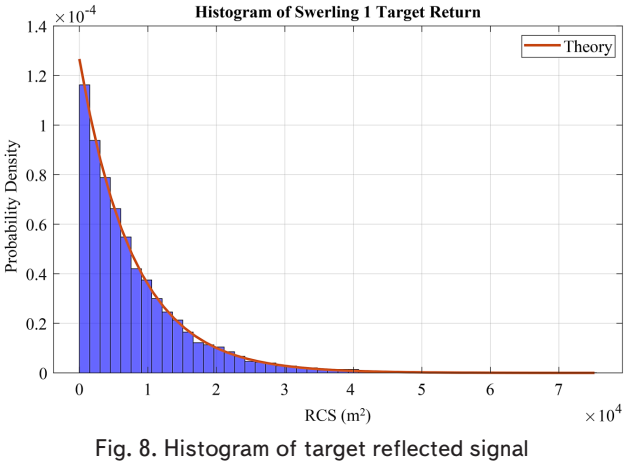

Fig. 8. Histogram of target reflected signal of Swerling 1 pattern

The histogram indicates that the reflection in the Swerling 1 is no longer constant. From scan to scan, the RCS value changes. We replicate the signal reflected energy for 10,000 scanning for an incident signal with unity value in a simulation, supposing the target was lit by the signal one time each dwell.

6. Discussion of the results of the work implementation of the radar cross-sections model

For the purpose of simulating a radar system, this work provided a basic introduction to radar target modeling. It demonstrated the modeling of point targets, measured targets' profiles, and extended targets. It also explained how to produce target echoes while accounting for statistical volatility. From the relation between RCS and elevation angle variations for a cylindrical target shown in Fig. 4, the obtained result was [88.8577 88.8577 1.3161]. This demonstrates that the first two outputs are the same and confirms that there is no azimuth angle dependence.

The nulls in the target's RCS pattern between 40 and 50 degrees azimuth are substantially shallower. When signals combine violently at a given azimuth and frequency, the narrowband pattern experiences deep nulls. This was shown in Fig. 7, which compares wideband and narrowband RCS patterns at zero elevation of 4 scatterers' extended target characteristics. Plotting the histogram output from every scan serves to confirm that the distribution of the output is matched with the theoretical estimation. This was indicated in Fig. 8, where the histogram of the target reflected signal of the Swerling 1 pattern was visualized.

The RCS profiles of 4 scatterers for an extended target are shown in Fig. 5 and have been utilized in the previously created radar *Target* object to calculate the reflected power of the target signals. This result confirms that the signal reflected power relies on both angles of elevation and azimuth directions.

The presented work didn't discuss the impact of polarization on target RCS. A single RCS number is no longer adequate to represent a target's polarization signature. Instead, a scattering matrix is utilized to explain how the target interacts with the polarization components of the incoming signal at each incident angle and frequency. Therefore, it is recommended to discuss such a case in future work.

7. Conclusions

1. Only elevation angle has an impact on RCS readings when visualizing RCS patterns for a cylindrical target. The obtained result confirms that there is no azimuth angle dependence.

2. The analysis of 4 scatterers' RCS for extended targets shows that the signal reflected power relies on both angles of elevation and azimuth directions.

3. The comparison between wideband and narrowband RCS patterns at zero elevation for 4 scatterers' extended targets demonstrates that the RCS profiles of the target were with much shallower nulls for azimuth direction in the range of (40–50) degrees.

4. The application of the target fluctuation case demonstrates that the RCS histogram of the target reflected signal of all scans agrees with the theoretical estimates. The histogram of the target reflected signal of the Swerling 1 pattern converges to approximately zero on about 5 m^2.

Conflict of interest

The authors declare that they have no conflict of interest in relation to this research, whether financial, personal, authorship or otherwise, that could affect the research and its results presented in this paper.

Acknowledgments

The authors would like to express their deepest gratitude to the University of Technology Baghdad-Iraq for their support to complete this research.

References

1. Semkin, V., Haarla, J., Pairon, T., Slezak, C., Rangan, S., Viikari, V., Oestges, C. (2020). Analyzing Radar Cross Section Signatures of Diverse Drone Models at mmWave Frequencies. IEEE Access, 8, 48958–48969. doi: https://doi.org/10.1109/access.2020.2979339
2. Tian, Z.-F., Wu, D., Hu, T. (2022). Theoretical study of single-photon quantum radar cross-section of cylindrical curved surface. Acta Physica Sinica, 71 (3), 034204. doi: https://doi.org/10.7498/aps.71.20211295
3. Sengupta, S., Council, H., Jackson, D. R., Onofrei, D. (2020). Active Radar Cross Section Reduction of an Object Using Microstrip Antennas. Radio Science, 55 (2). doi: https://doi.org/10.1029/2019rs006939
4. Zhang, T., Zeng, H., Chen, R. (2019). Simulation of Quantum Radar Cross Section for Electrically Large Targets With GPU. IEEE Access, 7, 154260–154267. doi: https://doi.org/10.1109/access.2019.2947738
5. Rajyalakshmi, P., Raju, G. S. N. (2011). Characteristics of Radar Cross Section with Different Objects. International Journal of Electronics and Communication Engineering6 4 (2), 205–216. Available at: https://www.ripublication.com/irph/ijece/ijecev4n2__6.pdf
6. Shi, W., Zhang, X., Shen, Y., Chen, H., Yu, Z. (2021). RCS Estimation and Synthesis of Typical Traffic Participants. 2021 Photonics & Electromagnetics Research Symposium (PIERS). doi: https://doi.org/10.1109/piers53385.2021.9694942
7. Dallmann, T., Heberling, D. (2014). Discrimination of scattering mechanisms via polarimetric rcs imaging [measurements corner]. IEEE Antennas and Propagation Magazine, 56 (3), 154–165. doi: https://doi.org/10.1109/map.2014.6867696
8. Alberga, V. (2004). Volume decorrelation effects in polarimetric SAR interferometry. IEEE Transactions on Geoscience and Remote Sensing, 42 (11), 2467–2478. doi: https://doi.org/10.1109/tgrs.2004.837330
9. Shijer, S. S., Sabry, A. H. (2021). Analysis of performance parameters for wireless network using switching multiple access control method. Eastern-European Journal of Enterprise Technologies, 4 (9 (112)), 6–14. doi: https://doi.org/10.15587/1729-4061.2021.238457

10. Al-Shoukry, S., M. Jawad, B. J., Musa, Z., Sabry, A. H. (2022). Development of predictive modeling and deep learning classification of taxi trip tolls. Eastern-European Journal of Enterprise Technologies, 3 (3 (117)), 6–12. doi: https://doi.org/10.15587/1729-4061.2022.259242
11. Li, M., Xiang, Y., Chen, X., Wang, Y., Lu, Y., Ding, Z. (2019). Altitude ambiguity suppression method based on dual-frequency interfering and multi-frequency averaging for sparse baseline TomoSAR. Electronics Letters, 55 (22), 1194–1196. doi: https://doi.org/10.1049/el.2019.2198
12. Ning, C., Lü, M., Gao, C., Wan, H. (2021). Clutter Reduction Method for Radar Cross Section (RCS) Measurement Based on InSAR Principle. Beijing Ligong Daxue Xuebao/Transaction of Beijing Institute of Technology, 41 (08). doi: https://doi.org/10.15918/j.tbit1001-0645.2021.024
13. Margarit, G., Mallorqui, J. J., Fortuny-Guasch, J., Lopez-Martinez, C. (2009). Exploitation of Ship Scattering in Polarimetric SAR for an Improved Classification Under High Clutter Conditions. IEEE Transactions on Geoscience and Remote Sensing, 47 (4), 1224–1235. doi: https://doi.org/10.1109/tgrs.2008.2008721
14. Lee, K.-C. (2019). Radar target recognition by frequency-diversity rcs together with kernel scatter difference discrimination. Progress In Electromagnetics Research M, 87, 137–145. doi: https://doi.org/10.2528/pierm19101201
15. Deep, Y., Held, P., Ram, S. S., Steinhauser, D., Gupta, A., Gruson, F. et. al. (2020). Radar cross-sections of pedestrians at automotive radar frequencies using ray tracing and point scatterer modelling. IET Radar, Sonar & Navigation, 14(6), 833–844. doi: https://doi.org/10.1049/iet-rsn.2019.0471
16. Baldauf, J., Lee, S.-W., Lin, L., Jeng, S.-K., Scarborough, S. M., Yu, C. L. (1991). High frequency scattering from trihedral corner reflectors and other benchmark targets: SBR versus experiment. IEEE Transactions on Antennas and Propagation, 39 (9), 1345–1351. doi: https://doi.org/10.1109/8.99043
17. Skolnik, M. I. (2008). Radar Handbook. McGraw Hill, 1328.
18. Youssef, N. N. (1989). Radar cross section of complex targets. Proceedings of the IEEE, 77 (5), 722–734. doi: https://doi.org/10.1109/5.32062